JOURNAL OF PROPULSION AND POWER
Vol. 17, No. 6, November–December 2001

Numerical Research of Gaseous Fuel Preinjection in Hypersonic Three-Dimensional Inlet

O. V. Guoskov,* V. I. Kopchenov,† K. E. Lomkov, and V. A. Vinogradov†
Central Institute of Aviation Motors, 111500, Moscow, Russia
and
P. J. Waltrup‡
Johns Hopkins University, Applied Physics Laboratory, Laurel, Maryland 20723

Numerical results of gaseous ethylene and propane fuel preinjection in a hypersonic three-dimensional inlet and the attendant fuel–air mixing enhancement process are analyzed. Fuel is injected in the wake of thin swept pylons located on the inlet's compression surface (installed normal to the wall), 1–2 injector diameters downstream of the pylons. Mixing in the near vicinity of the pylons is calculated using the Favre-averaged Navier–Stokes equations for three-dimensional, turbulent, multispecie, nonreacting flows, taking into account all of the jets. Calculations of the flowfield in the far mixing region of the inlet channel are based on solutions of the parabolized Navier–Stokes equations. It is shown that fuel–air mixing efficiencies between 0.95 and 0.98 are possible for fuel–air equivalence ratios between 0.3 and 0.7 before exiting an inlet channel whose length is 0.65 m.

Nomenclature

d	=	fuel injector diameter
$\bar{F}$	=	inlet area contraction ratio
G	=	mass flow
$H_{\max}$	=	maximum penetration height
L	=	distance from engine entrance
M	=	Mach number
P	=	pressure
S	=	pylon base width
T	=	temperature
X, Y, Z	=	Cartesian coordinates
β	=	fuel–air equivalence ratio
η	=	mixing efficiency
μ	=	molecular mass
φ	=	mass flow capture ratio coefficient
σ	=	inlet total pressure recovery

Subscripts

d	=	injector location
f	=	fuel parameters
t	=	total parameters
th	=	inlet throat parameters
Σ	=	averaged over cross section
∞	=	freestream parameters

Introduction

ONE of the problems affecting efficient combustion in high-velocity airbreathing engines is mixing of the fuel and air streams before combustion stabilization. This problem is applicable to hydrogen-fueledengines and even more so to gaseous- and liquid-hydrocarbon-fueledengines because of the increased complexity of the chemical kinetics and vaporization time for liquids.

The ideal situation is when a perfectly premixed fuel–air mixture with minimal total pressure loss is produced. To date, many different ways of fuel injection have been investigated,[1] each of which presents a different method for fuel–air mixing enhancement at or near the entrance of the combustor. The general principle of mixing enhancement over short axial distances is to create vortical or separated flows. However, these can lead to substantial impulse losses in the fuel–air stream via total pressure losses. The increased combustor length needed for effective mixing will also result in wall friction impulse losses, plus additional weight and structural fuel cooling requirements.

Typical fuel injection and mixing schemes for supersonic combustors include normal and angled injection from the flow channel wall or from an in-stream pylon wall, coflowing (axial) injection from the base of a reverse step or the base of an in-stream pylon, and combinations thereof. However, wall injection requires a rather large supply pressure, and pylon injection is accompanied by additional total pressure losses caused by the pylon aerodynamic drag and internal construction complexity for gas injection passages and active cooling requirements.

In addition to supersonic combustion ramjets, another engine cycle, the pulse detonation, engine, mandates that uniform fuel–air mixtures enter its combustor to produce thrust efficiently. However, to date, specific ways of providing this uniform mixture have not been clearly identified.

One way to overcome, in part, these deficiencies is to inject some or all of the fuel (in the limit case) before the flow enters the combustor, that is, in the inlet channel or on the nose of the inlet forebody. Whereas this requires more inlet–combustor integration, and strategic placement of the fuel to minimize the potential for preignition via the inlet forebody boundary layer, it should also provide a high degree of fuel–air premixedness before the flow entering the combustor.

Note that the idea of inlet fuel injection and combustor integration was considered in the scramjet engine concept for the X-30 (National Aerospace Plane) vehicle.[2] Here, a large portion of the fuel was to be injected from in-stream struts downstream the inlet throat well before the combustor entrance. These struts were simultaneously used as compression elements for deceleration of the incoming inlet airflow.

It is natural that one should be sure there will be no flame propagation upstream (danger of flashback) for all flight regimes during engine operation and, consequently, that the inlet will operate in all flight regimes without unstarting it. Moreover, fuel injection in the

Received 21 October 2000; revision received 29 August 2001; accepted for publication 29 August 2001. Copyright © 2001 by the American Institute of Aeronautics and Astronautics, Inc. Under the copyright claimed herein, the U.S. Government has a royalty-free license to exercise all rights for Govermental purposes. JHU/APL reserves all proprietary rights other than copyright; the author(s) retain the right of use in future works of their own; and JHU/APL reserves the right to make copies for its own use, but not for sale. All other rights are reserved by the copyright owner.

*Research Scientist.
†Head of Sector. Member AIAA.
‡Senior Engineer/Scientist. Associate Fellow AIAA.

inlet could be used to produce some of the required compression of the incoming airflow traditionally generated by inlet compression surfaces and for preheating the fuel using the heated airstream as the energy source. At the same time, it follows that this precombustor fuel injection will enhance the secondary breakup of fuel droplets and enhance fuel–air mixing in the case of liquid fuel injection due to interactions with the inlet's multishock compression system.

Liquid injection in supersonic airflow has been investigated in an earlier study,[3] where liquid kerosene was injected into a supersonic Mach 2–4 airflow behind a thin swept pylon. One of the main results of this research[3] was that the required depth of fuel penetration was achieved using kerosene dynamic pressures equal to or less than the dynamic pressure of the airflow, whereas fuel injection in combustors requires fuel dynamic pressures several time those of the airstream.

An example of liquid injection in a supersonic inlet in an $M_\infty = 3.5$ freestream airflow is presented in Ref. 4. In this study, a liquid injectant, mixture of 50% by volume commercial ethylene glycol in water, whose viscosity and surface tension were representative of JP-10 fuel, was injected in a two-dimensional inlet through orifices oriented normal to the compression surface in the wake behind each of two swept pylons of triangular cross section. It was found that the flowfield in the inlet remained started with only minor separated regimes using liquid injection rates corresponding to fuel–air equivalence ratios for kerosene of $\beta \leq 0.45$, and practically all of the liquid injectant was situated in the core of the flow, which is favorable for prevention of upstream flame propagation. This conclusion is based on previous experimental measurements.[3,4]

Another experimental study supporting the argument that flashback through the boundary layer can be prevented even with a small amount of liquid fuel present in the boundary layer is presented in Ref. 5. In this study, tests were conducted on a 250-mm-diam axisymmetric dual-mode scramjet model at $M_\infty = 6.2$ with air total temperatures and pressures between $T_{t\infty} = 1400$ and 1600 K and $P_{t\infty} = 4.8$ and 5.5 MPa, respectively. Liquid kerosene at rate equal to $\beta_{\text{ker}} = 0.4$–0.45 was injected normally to the flow direction on the inlet's conical surface located 20 mm downstream of its apex through six orifices of 0.5 mm diam. For combustion initiation and stabilization, gaseous hydrogen was injected in the front section of the cavity flameholders located downstream of the inlet on both the inner and outer (cowl) walls at the entrance of an annular supersonic combustion chamber. After ignition of the hydrogen by the spark plugs and flame stabilization, kerosene was injected 2–3 s later and was ignited and sustained by the products of the hydrogen combustion. The quantity of hydrogen injected was small ($\beta_{\text{H2}} = 0.15$–0.2), the amount of which was experimentally determined for stable operation of the flameholder. When hydrogen injection was stopped, however, combustion of the kerosene stopped as well. This last observation can be explained in that there was insufficient kerosene from the upstream inlet fuel injection captured by the cavities (from fuel injected through and captured in the wall boundary layer) to initiate or sustain combustion either through flame propagation or a residual flame.[6]

Successful application of this methodology has also been demonstrated in research on external burning (or combustion) with the aim of obtaining aerodynamic forces acting on a vehicle for vehicle control, increasing lift, and/or decreasing forebody or aftbody vehicle drag.[7]

Consequently, normal injection of a gaseous-hydrocarbon fuel injected in the wake behind thin swept pylons placed on an inlet channel wall was chosen for this research and as an alternate for comparison with normal wall fuel injection without the pylons present. Also, to improve the macromixing processes and fuel–air homogenization, some of the fuel could also be initially injected at supersonic speeds on the internal surfaces of the inlet just downstream of its leading edge. Finally, for the given method of sonic or supersonic gaseous fuel injection, the pylon thickness must be of the same order as the gas injector diameter, and the penetration height (injector pressure) is determined by the need for fuel in a given region of the channel cross section.[3]

The pylon's length is defined by the material's heat absorption capabilities and conductivity and the amount of convective cooling its base provides coupled with the gas spray fuel plume. Furthermore, the pylons have a small thickness, and, therefore, their drag is equivalent to or no more than the pylon drag of thickness equal to the thickness of an unprotected fuel jet injected in a supersonic flow. The concomitant cooling requirements will be minimal based on unpublished data. In fact, proper arrangement of the pylons on the inlet compression surfaces may remove any active cooling requirements. In this case, the simplicity of fuel injection through the orifices is also retained.

Task Formulation and Computational Technology

The primary purpose of these investigations is to evaluate the possibility and potential of premixing part of the fuel when it is injected in the air inlet before the isolator duct and combustion chamber. The primary question addressed at this stage of the study is the proper choice and design of the fuel injection system in the inlet. In subsequent studies, it is proposed to study, in more detail, the influence of the partially premixed fuel–air on the potential for preignition of this mixture in the inlet/isolator ducts and ignition and combustion in combustor where the remainder of the fuel is injected.

The inlet chosen for study is a three-dimensional, fixed geometry configuration consisting of two opposed, swept wedged walls arranged on a flat base and covered by a cowl in the rear part, as shown in Fig. 1. This inlet is a half width version (divided at the symmetry plane) of one considered for use in the Oryol-2 program, and it has been tested between Mach 2 and 6 (Ref. 8). Figure 2 is a photograph of the inlet tested and subsequently integrated into a freejet engine model. Note that the results of this study are planned for incorporation in planned tests of this engine in the Institute of Theoretical and Applied Mechanics hot-shot impulse wind tunnel.

For the current study, the side wall inlet compression wedge angle is 6 deg, and the central strut wall wedge angles are a 4-deg initial angle followed by 2 deg more compression (for a total of 6 deg). These angles were chosen to permit starting of the inlet and efficient deceleration and compression of the incoming flow at Mach 6–8. The aft strut compression leading-edge sweep and the side wall

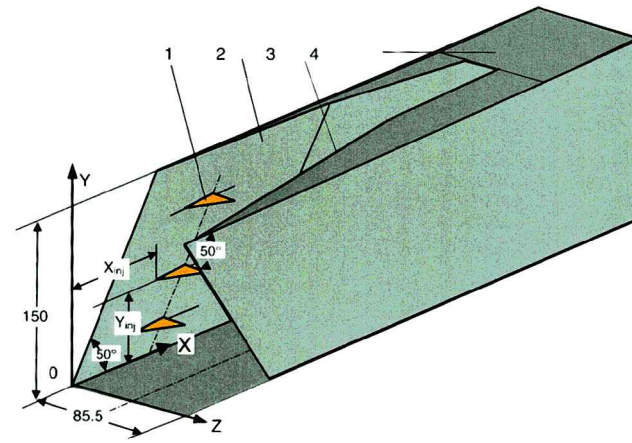

Fig. 1 Schematic of fuel pylons installed in the inlet: 1, pylon/fuel injector; 2, central strut wall; 3, side wall; and 4 cowl.

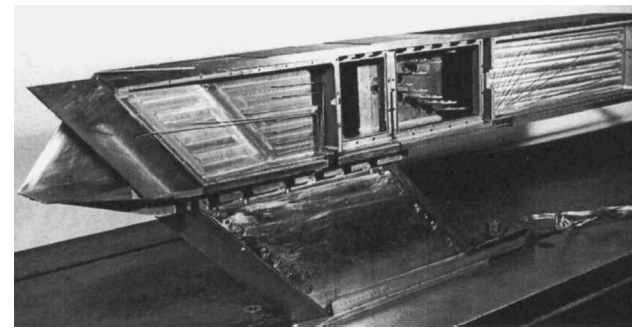

Fig. 2 Dual mode scramjet freejet model.[8]

Table 1 Pylon/fuel jet penetration parametric cases

			Air						
Case	S/d	X_d/d	$P_{t\infty}$, bar	T_t, K	M_∞	T_{tf}, T_f, K	P_{tf}, bar	Fuel	Comments
1	1.5	2	100	2000	6	300	3	C_2H_4	With pylon
2	1.5	1	100	2000	6	300	3	C_2H_4	With pylon
3	1.5	3	100	2000	6	300	3	C_2H_4	With pylon
4	2	2	100	2000	6	300	3	C_2H_4	With pylon
5	1	2	100	2000	6	300	3	C_2H_4	With pylon
6	——	2	100	2000	6	300	3	C_2H_4	Without pylon
7	1.5	2	100	2000	6	300	3	C_2H_4	Taking into account wall boundary layer
8	1.5	2	100	2000	6	300	5.67	C_2H_4	With pylon
9	1.5	2	100	2000	6	300	6.2	C_3H_8	With pylon
10	1.5	2	300	2500	8	300	4.1	C_3H_8	With pylon

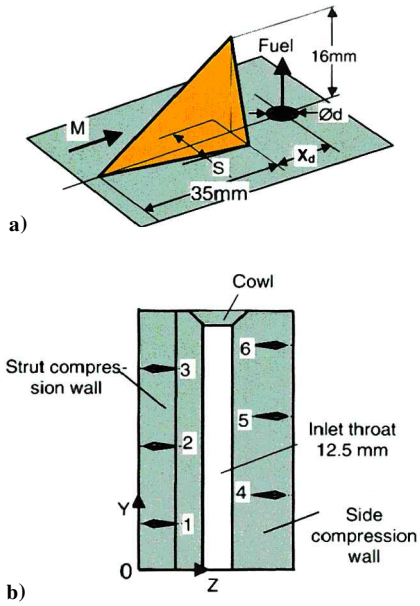

Fig. 3 Schematic of gas injection behind the pylon: a) installation of pylons in inlet channel (front view) and b) 1–6 numbers of pylons, s/d = 1.5, x_d/d = 2, and d = 3.4 mm.

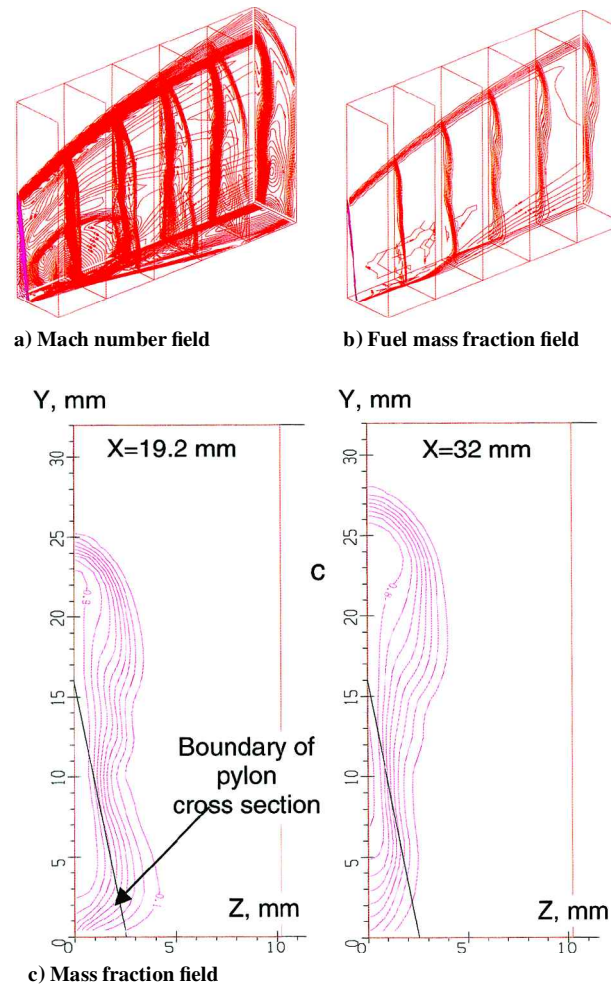

Fig. 4 Flowfield behind the pylon with fuel injection (case 8, β_f = 0.73, Table 2).

compression forward leading-edge sweep plus the rear position of the cowl provide effective air bypass area for inlet starting without using a variable geometry structure. In addition, the effective inlet-throat-to-inlet-geometric area ratio (relative inlet throat area $\bar{F}_{\text{th}}$) was decreased to $\bar{F}_{\text{th}} = 0.2$ compared with $\bar{F}_{\text{th}} = 0.4$ for the inlet as previously tested.[8] Here inlet geometric area is the projected frontal area of the inlet. The length of the side panels were also redesigned in such a manner that the distance from the inlet entrance ($X = 0$) to the throat section (0.49 m) was minimized, and the cross section was located on the inlet centerline.

An example of an air inlet pylon, fuel preinjection scheme considered in this study is shown in Fig. 3. Here, three fuel pylons are staggered on each of the lateral wedge surfaces of the inlet (Fig. 1), with all dimensions given in millimeters. All of the pylons have a triangular cross section with a 24.5 deg swept leading edge. Gaseous fuel is injected through 3.4-mm sonic orifices oriented normal to the inlet surface and located directly behind each pylon. The position of each pylon is such that the flow is undisturbed by the flow structure from another pylon at either Mach 6 or 8. Normal injection of the same number (and location) of fuel jets from the lateral inlet walls without the presence of pylons is considered as a comparative alternative to the pylon injection case.

Two computational tasks are considered necessary to evaluate the mixing efficiency of the investigated inlet fuel preinjection schemes. The first is the calculation of the flowfield generated by the sonic, normal wall fuel injection behind an individual fuel pylon. The numerical solution of this first task is performed using Favre-averaged full Navier–Stokes (FNS) equations for three-dimensional turbulent flows of multispecie mixtures.[9] The turbulence model used is the differential one-parameter model in Ref. 10. Multi-specie, gaseous-hydrocarbon fuel in thermochemical equilibrium is assumed.

The second computation determines the number and optimum location (or relative positions) of individual pylons to maximize fuel–air mixing efficiency for a given fuel–air equivalence ratio. For this second task, the supersonic flow in the duct is calculated using the parabolized Navier–Stokes (PNS) equations for turbulent flow of gas mixtures, and the wall boundary layer is ignored. The last assumption was accepted after the preliminary calculations for the first task in Tables 1 and 2 showed that the effect of the boundary layer on flowfield pattern and jet penetration was rather small. The

numerical method is based on the modification[11] of the steady analogy of the Godunov et al. scheme[12] for supersonic flows. Integral conservation laws are written for each computational cell. The problem of the interaction of two semi-infinite supersonic flows is used to find convective fluxes through the lateral faces of each cell. The higher-order accuracy and monotonicity of the scheme are achieved using the minimal derivatives principle and a predictor–corrector scheme, which result in minimization of the number of iterations needed to achieve a solution.

However, in-stream turbulence and equilibrium but nonreactive hydrocarbon fuel and air specie concentrations are accounted for in the calculations. Solutions of the flowfield downstream of each of the pylon/wall fuel injectors are then superposed on the PNS flowfield to define a new initial profile for additional PNS calculations up to the exit of the inlet.

For the first task, the airflow at the end of the cross section of the backward face of a given strut is assumed to be uniform and undisturbed by the pylon, that is, the uniform airstream parameters for the first computation are chosen as the ones behind the shock generated by the lateral wedges of the inlet. The distance from the base face of the pylon to the fuel jet centerline along with the width of the triangular base for a fixed pylon height is then varied. The goal of these calculations is to choose the jet injection axial location that provides both maximum fuel jet penetration into the airstream and maximum mixing efficiency. The computations are continued downstream until the normally injected fuel jet turns parallel with the main airstream direction and becomes supersonic in the axial direction.

Table 2 Fuel jet penetration for fuel mass fraction of 0.1 for Table 1 cases

Case	H_{max}, mm	Rams ratio
1	22.7	0.377
2	22.8	0.377
3	22.85	0.377
4	22.0	0.377
5	23.5	0.377
6	6.95	0.377
7	22.3	0.377
8	25.2	0.713
9	26.6	1.061
10	25.1	0.761

Solutions downstream of each of the pylon/normal wall fuel injector locations (sometimes referred to as fragment of the flowfield) are then stored so that they can latter be integrated with (or superposed on) PNS solutions of the initial inlet flowfield. The transverse and lateral dimensions of the fragments are chosen such that individual fragments do not interact with one another and with the wall boundaries.

Determining the relative positions of the fuel pylon/normal wall injector locations on the lateral inlet wedges that provide maximum integrated mixing efficiency comprises computational step 2. Here, mixing efficiency is defined as the potential ability of the calculated fuel–air mixture to burn completely using one ideal global reaction, for example, $C_2H_4 + 3O_2 = 2CO_2 + 2H_2O$, in accordance with the fuel and inlet air capture mass flows and specie concentrations. In computing the solution to this flowfield, it is necessary to take into account the actual duct geometry, fuel pylon and normal wall injector locations, and processor storage and computational speed.

The global flowfield in the duct having multiple pylon/fuel jet injection locations is obtained as follows. The supersonic flowfield, beginning at the entrance plane of the inlet duct, is calculated using the PNS equations, but without including the wall boundary layer. This method, however, allows taking into account the turbulent mixing process. At the axial location of the computed fragment of the flowfield (step 1) downstream of the pylon/fuel injector located nearest the inlet duct entrance, the actual flowfield fragment is inserted into the global cross-sectional flowfield. This fragment insert procedure is based on the assumptions that disturbances from individual fuel jets, including any shocks generated, do not reach the boundaries of other fragment regions and that the flow inside a given fragment region is not influenced by the external flow (into which the fragment is inserted). In other words, it is assumed that the two flowfields of interest, the PNS-calculated external, into which individual fragments are inserted, and in the FNS calculated internal regions, which are just the fragments, do not interact with one another up to the cross section where two solutions are matched.

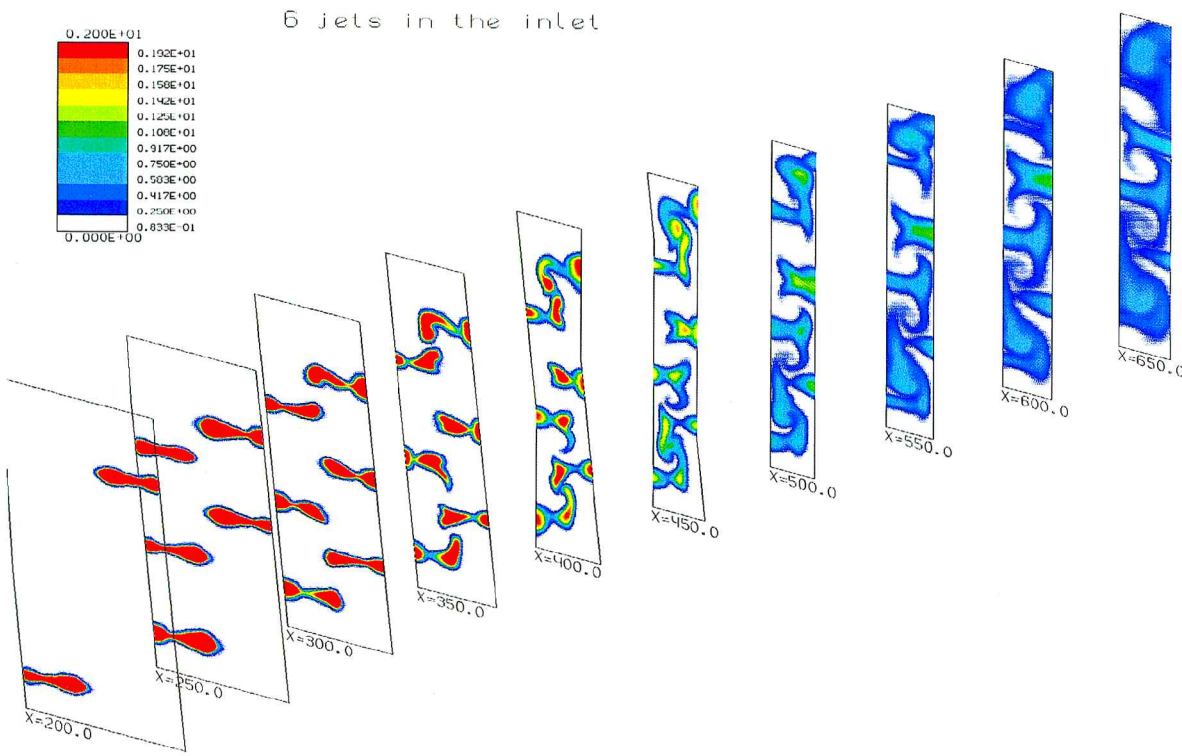

Fig. 5 Axial fuel distributions, β; case 3 (Table 5), ethylene pylon injection, β_Σ = 0.23.

Flowfields for additional pylon/fuel injectors located downstream of the first pylon are then patched to the reinitialized flowfield, which now includes the inlet (or external) plus any pylon/fuel injector flowfields preceding the one about to be included. This is accomplished by marching the PNS solution to the FNS solution for each additional pylon, reinitializing the cross-sectional flowfield data, and then marching downstream with the PNS solution until reaching the axial location of the next FNS-generated pylon fragmented flow solution.

Such a solution technique is implemented up to the end of the pylon/fuel injection region. As a result, a solution of the nonreacting, global flow picture can be obtained at the exit of the fuel injection region. Then the downstream solution is obtained for a given duct geometry and pylon/injector geometric pattern without taking into account wall boundary layer up to the exit of the inlet duct section. Note that this method of solving the flowfield takes into account the turbulent mixing of the injected jets with the airstream and permits evaluation of the mixing efficiency including the effects of a real, complex flow structure including the inlet's shock system.

Of course, the computational process used is an approximate one because the inserted fragments of the flow were obtained for individual isolated systems, on backward-facing pylon bases/steps with downstream normal wall jets placed in a uniform airstream. Also note that the procedure used for obtaining solutions to the pylon/fuel jet and inserting it into a global flow becomes increasingly more approximate as one moves in the downstream direction, especially when considering the increasing complexity of the real flow structure with axial (and lateral) distance as the number and location of pylon/fuel injectors increases.

However, this computational process (technology) was conceived to allow, as a first approximation, an inexpensive, computationally nonintensive, comparative analysis of the mixing efficiency achievable with various numbers and locations of pylons and their associated fuel injectors. Undeniably, the interaction of one pylon/fuel injector flow element with the flow fragment of another can and will appear in an actual flowfield.

Analysis of the Flow Behind the Pylon with Fuel Injection

The task of computing the injection of a gaseous, normal, sonic fuel jet from the wall in the base region of a triangular pylon is considered. A schematic of the pylon and fuel jet is shown in Fig. 3a. The computational region can be represented by a rectangular parallelepiped, whose left boundary is positioned at the cross section of pylon's back face. In the calculations presented later, this axial location (or cross section) corresponds to the coordinate $X = 0$. The right boundary was at an axial cross section of $X = 32$ mm. The height of computational region also equaled 32 mm. It is also assumed that the flow is symmetrical relative to the vertical symmetry plane of the pylon. Therefore, one computational boundary coincided with the plane of symmetry, and only half of considered region was computationally computed.

Uniform flowfield parameters, corresponding to the flow behind an oblique shock generated by airflow over 6-deg wedge, were set as the initial conditions for the FNS solution of the pylon/normal wall fuel injector flowfield. The effects of the flow over the strut were not taken into account. The no-slip condition for velocity was imposed on the strut backface, and the slip condition was imposed at the lower wall boundary (except in the region of the jet). In the case when the boundary layer was accounted for, the no-slip conditions were set at the lower surface. The conditions of the drift (known boundary conditions on the control volume) of all disturbances were set at the exit boundary, that is the no-reflection condition was set at the upper (freestream) boundary, and the condition of symmetry was set at the lateral sides. A large part of the calculations was computed on a grid containing $50 \times 40 \times 40$ cells because this value is close to maximal for the personal computer used (Pentium II processor). The calculations, which included the boundary layer on the lower wall where the sonic fuel injector orifice was located, were executed using a $50 \times 60 \times 40$ grid.

The calculations were performed with the code FNAS3D developed at the Central Institute of Aviation Motors for the calculation of three-dimensional viscous flows with multigas specie. The program

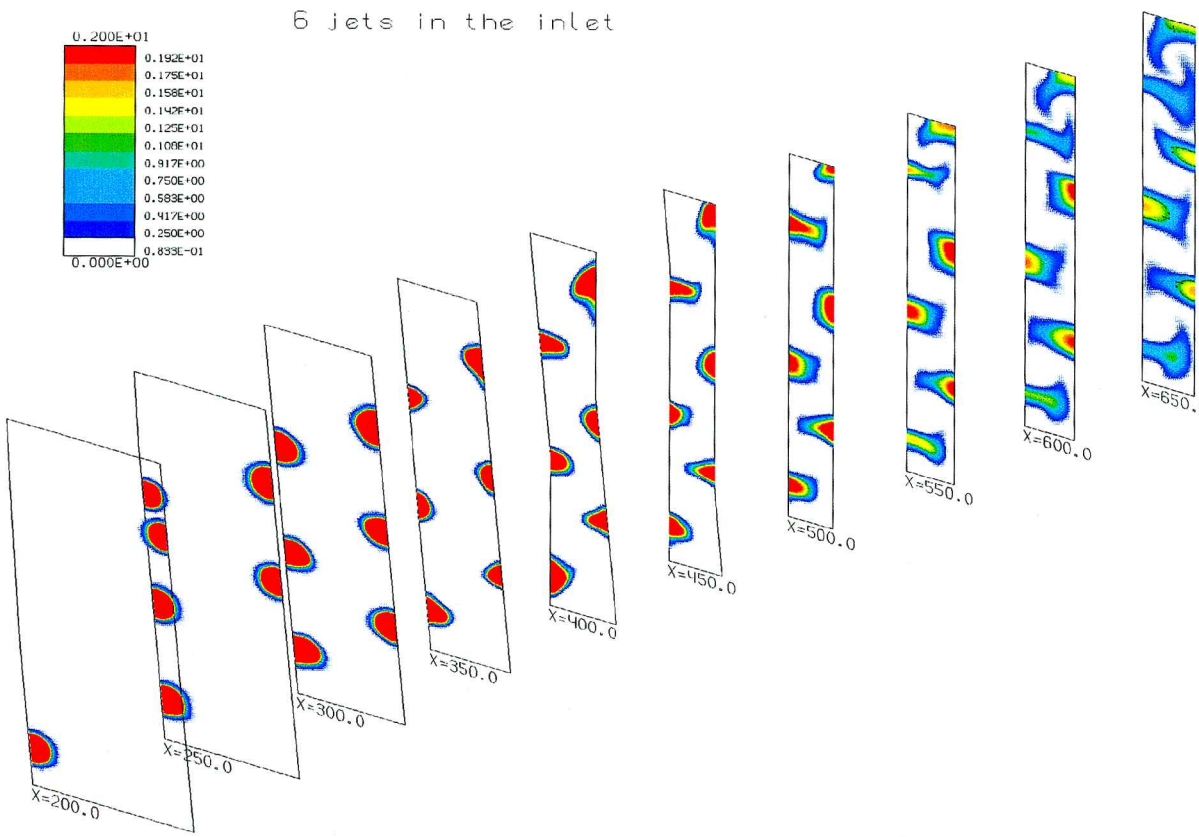

Fig. 6 Axial fuel distributions, β; case 5 (Table 5), ethylene wall injection (no pylons), $\beta_\Sigma = 0.23$.

is based on the integration of the full averaged system of Navier–Stokes equations using the time relaxation procedure and implicit finite difference scheme. The one-parametric model for turbulent viscosity is used for problem closing.[10] This code is the further development of FNAS2D[9] for two-dimensional and axisymmetric viscous turbulent flows containing multichemical specie taking into account chemical kinetics. The finite difference scheme used in this code is a modification of the Godunov et al. scheme.[12]

A series of parametric pylon/ethylene fuel injector calculations were conducted using this computational method. The main parameters and geometric variations considered are listed in Table 1. In the first five cases, the ratio of the maximum pylon base (backface) width-to-injectorjet diameter S/d, and the distance of the jet center from the pylon back face X_c/d were varied, with the parameters of the inlet air and fuel jet remaining constant. The results of the calculations show that the changes listed for these geometric parameters have no pronounced effect on the flow pattern. Therefore, the geometry corresponding to case 1 was chosen as the base geometry.

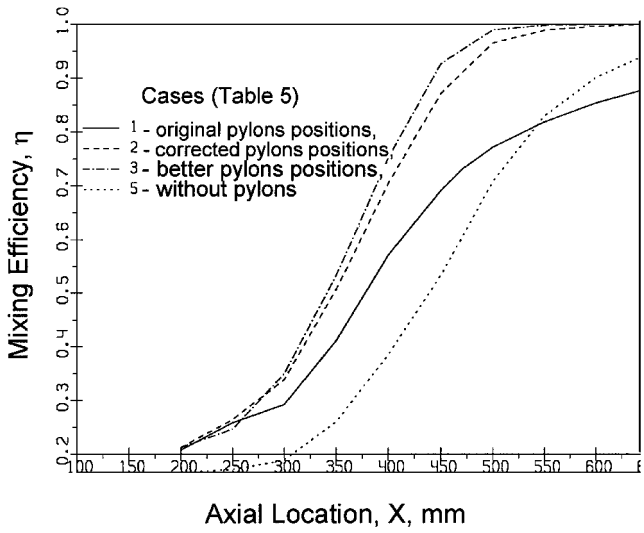

Fig. 7 Mixing efficiency for C_2H_4 injection at $M_\infty = 6$.

To show influence of the presence of the pylon on the jet penetration height, case 6, where the wall fuel jet was injected directly into the freestream, was considered. In case 7, the influence of the lower wall boundary layer development on the flowfield was calculated. This boundary layer approximated the boundary layer on a flat plate at a distance of 100 mm from the plate's leading edge. These calculations show that accounting for the wall boundary layer results in a minimal change in the flow pattern near the wall and practically no effect on the jet penetration depth into the flow.

In case 8, the fuel supply pressure and, accordingly, fuel mass flow were increased. In cases 9 and 10, the ethylene was replaced by propane. At the same time, in case 9 the total pressure of the fuel jet was also increased (from 3 to 6.2 bar). Finally, to determine the effect of flow Mach number on the results, the airflow Mach number in case 10 was increased from 6 to 8.

An example of the pylon/fuel injector calculations is presented in Fig. 4. The flow patterns in the near region behind the strut are shown by plotting Mach number and fuel mass fraction cross-sectional flowfields at several axial locations and fuel mass fraction cross sections at $X = 19.2$ and 32 mm. The step between lines of constant value for all flowfields is 0.1. The values of maximum height H_{max} of the constant fuel concentration 0.1 line above the injection wall at cross section $X = 19.2$ mm are presented in Table 2 for each of the 10 cases listed in Table 1. This value allows one to estimate the depth of fuel penetration into the airflow. The dynamic pressure (rams) ratio of the fuel and airflow ahead the pylon are also presented in Table 2 for these same 10 cases.

Based on the results in Tables 1 and 2 plus Fig. 4, it is possible to conclude the following. 1) The depth of jet penetration does not significantly increase for the changes in geometry considered (size of the pylon base to injector diameter and distance from the strut backface to the fuel jet, cases 1–5). The maximum difference in fuel jet penetration based on a fuel concentration level of 0.1 does not exceed 7%. 2) The presence of the pylon results in a substantial increase in jet penetration depth at the same airflow and fuel jet parameters. This conclusion follows from a comparison of cases 1–5 on the one hand and case 6 on the other. 3) An increase in fuel delivery pressure and, concomitantly, fuel mass flow by a factor of 1.89 (cases 1 and 8 are compared) is accompanied by the increase in jet penetration depth of approximately 11%.

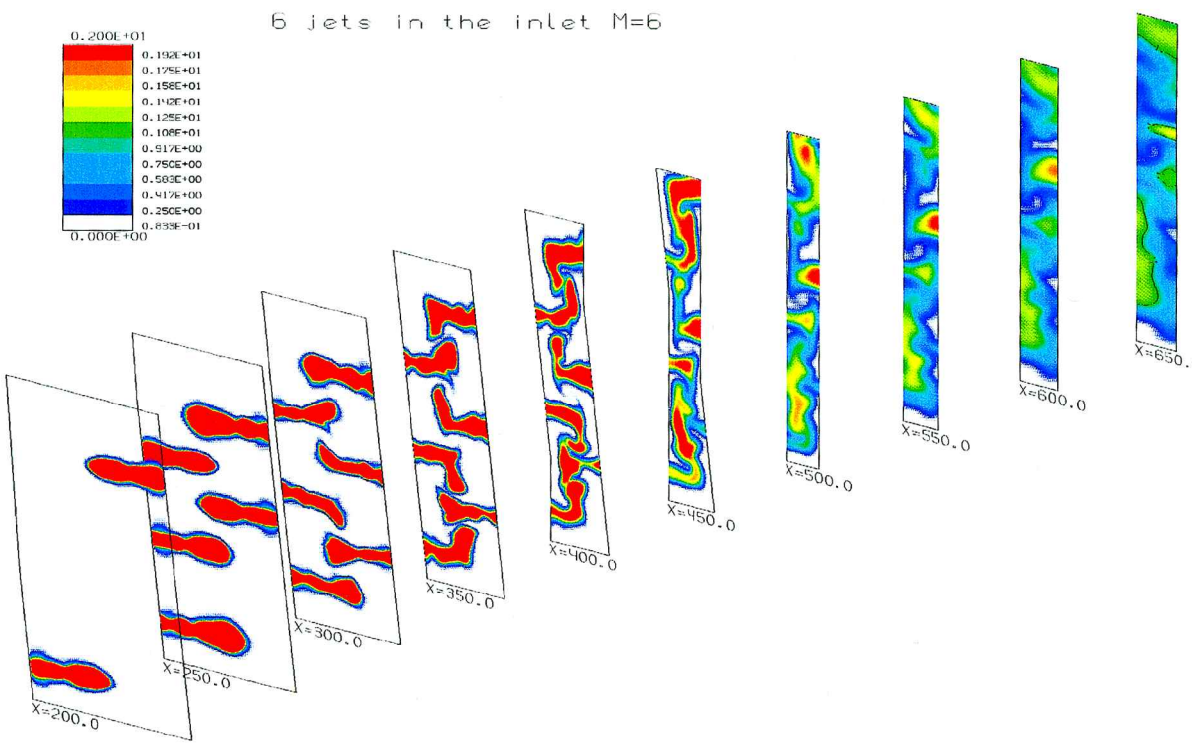

Fig. 8 Axial fuel distributions, β; case 6 (Table 5), propane pylon injection, $\beta\Sigma = 0.66$, and $M_\infty = 6$.

Note that the distribution of parameters at cross section $X = 19.2$ mm (where the flow on the boundaries is not perturbed yet, but the flow is already completely supersonic) were stored as the fragments needed for the complete flowfield solution (task 2 solutions).

Choosing Fuel Pylon Positions in the Inlet and Estimating the Mixing Efficiency

The choice of the fuel injector/pylons relative positions and the resulting mixing efficiency estimation are based on the second task solution. Because the first task computes the FNS flowfield in the vicinity of each pylon/fuel injector, the flowfield in the near field downstream of the strut, for example, at $L = 19.2$ mm from the strut base, is known. The flow in this cross section is supersonic (except in the wall boundary layer), and the known flow parameters can be used for calculating mixing in the downstream direction using the PNS marching procedure. The marching procedure starts at the inlet entrance section and is stopped every time it intersects a pylon/fuel injector FNS generated cross section at length L downstream of the next pylon base. In this cross section, the flow fragment known from the FNS solution replaces part of the airstream. This flow fragment insert includes the replacement of a section of the airstream with a fuel–air mixture. Within this procedure, the air concentration is changed so that sum of mass fractions is equal to 1. Then the marching step is continued.

Six pylons were chosen for this study because this arrangement resulted in a reasonably uniform fuel–air distribution at the inlet's throat. Furthermore, a four-pylon configuration analyzed was found to have less uniformity of the fuel–air mixture at the throat. No other attempts to optimize the number of pylons were made. The PNS equations for turbulent flow of gas mixtures are then solved and marched downstream to the next fragment. Once all of the fragments (or pylon/fuel injector flowfields) have been incorporated, then the solution is marched to the exit of the inlet duct, which is 0.65 m long for the current example.

Computations of the fuel–air mixing in the inlet have been performed for three initial variants. The first variant is the choice of the position of the six pylon/fuel injectors in the inlet duct to maximize uniformity of the fuel–air mixture at the exit of the inlet duct. All computations were done for an area contraction to the inlet throat of $\bar{F}_{\text{th}} = 0.2$. The air and fuel parameters are presented in Table 3, and the initial pylon positions are given in case 1 columns of Table 4. The calculated flowfields and resulting local fuel–air equivalence ratio β show that pairs of jets injected from opposite sides of the inlet interact with one another and limit fuel jet penetration into the airstream. That is why, in the next two cases (Table 4, cases 2 and 3), the pylons on the left side have been moved upstream by 8–15 mm. These new positions were chosen based on additional calculations for fuel–air distribution and mixing efficiency for several axial pylon positions. The corresponding local equivalence ratio β distributions for the final pylon/fuel injector positions (case 3) are shown in Fig. 5. These results show a rather uniform filling of the cross section with fuel by the exit of the inlet duct, and better mixing was calculated compared to the first two cases.

The two additional variants calculated for these pylon positions include case 4 in which the pylon/injector fuel–air or equivalence ratio was increased from approximately 0.25 to 0.47, and case 5, in which the flowfield for wall fuel injection without pylons present was computed. The β distributions for case 5 are shown in Fig. 6, which shows that the fuel jet penetration and inlet fuel–air mixing are substantially decreased in the absence of the pylons.

A quantitative evaluation of the mixing efficiency for each of the cases in Table 5 has also been estimated using the following process. In the cross-sectional area at a given $X = \text{const}$, the amount of fuel ready to be burned in a given computational cell is defined by the local fuel/air equivalence ratio. If $\beta \leq 1.0$, then it is assumed that the fuel–air mixture is ready to react. Summarizing the amount fuel ready for combustion over all cells at a given area cross section will yield the total amount of fuel ready to be burned. The ratio of this mass flow to the total fuel mass flow (if $\beta_{\text{total}} < 1$) is the mixing efficiency η. Curves for cases 1–3 and 5 from Table 5 are shown in Fig. 7. One can see that the mixing rate strongly decreases in case 1 after the opposing fuel jets merge. However, when the pylons are better staggered, as in cases 2 and 3 in Table 5, the mixing efficiency increases, reaching its maximum possible value at or before the exit of the inlet (at $X = 650$ mm). In case 5 (without pylons present), mixing is poor in the initial section of the inlet duct, then it becomes slightly more intensive, reaching a maximum value of 0.85. Increasing the equivalence ratio β from 0.26 to 0.47 at $M_\infty = 6$ decreases inlet total pressure recovery by $\approx$15%, but when the β increase is from 0.47 to 0.66, the total pressure recovery is decreased by $\approx$ 19%.

A final variant computationally investigated was to increase the inlet's geometric compression from $\bar{F}_{\text{th}} = 0.2$ to 0.15 and use different fuel (C_3H_8 vs C_2H_4) at a somewhat higher equivalence ratio (0.66 vs 0.25–0.47). In this case, the cowl leading edge was moved downstream to $X = 480$ mm. The pylon positions are almost identical to those in cases 3 and 4; the difference is that one strut has been moved downstream by 5 mm (see Table 4). Integral characteristics for these cases (6 and 7) are shown in Table 5.

Table 3 Two series of cases used for computations

	Air					Fuel, C_2H_4						
Series	M_∞	P_t, bar	$T_{t\infty}$, K	P_∞, bar	T_∞, K	M	T_{tf}, K	μ_{tf}	L_0	G_f, g/s	P_{tf}, bar	β_Σ
					$F_{th} = 0.2$, $L_{\text{cowl}} = 440$ mm							
1[a]	6	100	2000	0.0485	250	1	300	——	14.9	——	——	——
					$F_{th} = 0.15$, $L_{\text{cowl}} = 480$ mm							
2[b]	6	100	2000	0.0485	250	1	300	44	15.1	10.7	6.2	——
2[b]	8	300	2500	0.02	205	——	——	——	——	6.65	4.1	0.66

[a]Choosing of pylon positions. [b]Higher compression, more fuel.

Table 4 Pylon positions in different cases

	Case 1 (original)			Case 2		Cases 3–5		Cases 6 and 7 ($M = 6$, $M = 8$)	
N	X, mm	Y, mm	Z[a]	X, mm	Y, mm	X, mm	Y, mm	X, mm	Y, mm
1	111	25	0	103	15	103	15	103	15
2	151	70	0	139	55	139	55	139	55
3	186	115	0	178	105	174	100	170	95
4	184	35	1	184	35	180	40	180	40
5	147	80	1	147	80	147	80	147	80
6	110	125	1	114	120	114	120	114	120

[a]Sign of left/right wall (see Figs. 1–3).

Table 5 Cases and integral flow characteristics at inlet exit

Case	Comment[a]	Entry air mass flow ($X=0$)	Throat mass flow, kg/s ($X=650$)	φ	Entry fuel mass flow, g/s ($X=300$)	Throat fuel mass flow, g/s ($X=650$ mm)	$\varphi_\beta/\varphi_{\beta=0}$	β_Σ (throat)	σ	P/P_∞	M
0	Without pylons and injection	2.1637	1.9591	0.905	0	0	1.000	0	0.733	7.77	4.06
1	Original pylon positions	2.1637	1.972	0.911	40.40	40.2	0.995	0.3	0.549	9.07	3.72
2	Pylon position 2	2.1637	1.961	0.906	33.64	33.64	1.000	0.26	0.533	9.07	3.70
3	Pylon position 3	2.1637	1.959	0.905	32.14	32.14	1.000	0.24	0.527	9.09	3.696
4	More fuel	2.1637	1.941	0.897	60.47	60.45	1.000	0.47	0.448	9.74	3.53
5	With fuel, no pylons	2.1637	2.018	0.933	31.1	30.8	0.990	0.23	0.515	9.58	3.65
6	$F_{th}=0.15$	1.6277	1.367	0.840	60.8	59.95	0.986	0.66	0.36	14.81	3.096
7	$F_{th}=0.15$	0.9895	0.946	0.956	37.66	37	0.982	0.62	0.254	19.7	3.90

[a]Cases 0–6, $M_\infty=6$; case 7, $M_\infty=8$.

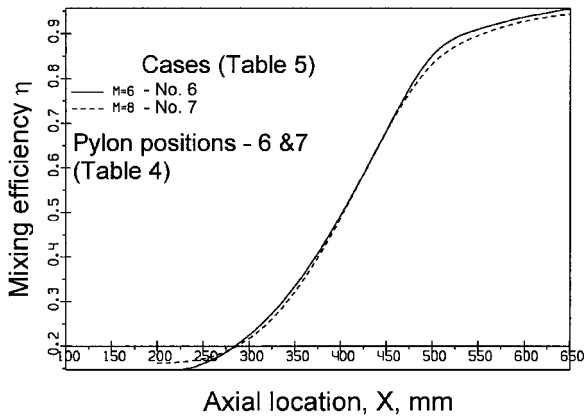

Fig. 9 Mixing efficiency for C_3H_8 injection at M_∞ = 6 and 8.

Computations were then made at $M_\infty=6$ and 8. An example of the local equivalence ratio distributions at $M_\infty=6$ and $\beta_\Sigma=0.66$ is presented in Fig. 8. Note that inlet air capture ratio φ is smaller than in the first series due to the higher compression and movement of the inlet cowl. Moreover, some of the fuel passes out of the duct, especially for $M_\infty=6$ (see Table 5). If necessary, this disadvantage can be overcome by rearranging the pylon axial positions. The corresponding curves of mixing efficiency given in Fig. 9 show that a mixing efficiency of only 0.95 is achieved at both Mach numbers. This efficiency is less than some of those shown in Fig. 7 primarily because the local fuel–air equivalence ratios are higher and the mixing is slower. Note that changing fuels has no discernable effect on mixing. In addition no inlet unstart was noted from mass addition for any case studied.

Summary

This study has demonstrated that normal injection of gaseous fuel in an air inlet from wall injectors located behind thin swept pylons enables sufficient penetration and complete mixing of the fuel before the exit of the inlet. A rationale for the choice of the pylon/fuel injector positions is suggested that can provide mixing efficiency levels up to $\eta=0.95$–0.98 at the inlet exit using fuel rates corresponding to fuel/air equivalence ratios of $\beta=0.25$–0.66.

To check some of the assumptions accepted in this research the authors propose to conduct mixing of air and fuel jets for simplified geometrical configuration, single pylon in a channel of constant cross-sectional area, and to compare with results by comprehensive numerical codes obtained. It is also proposed to conduct a study at low M_∞ (down to $M_\infty=3$).

Acknowledgment

John Hopkins University, Applied Physics Laboratory, supported this work.

References

[1]Seiner, J. M., Dash, S. M., and Kenzakovich, D. C., "Historical Survey on Enhanced Mixing in Scramjet Engines," AIAA Paper 99-4869, Nov. 1999.

[2]Henry, J. R., and Anderson, G. Y., "Design Considerations for the Airframe-Integrated Scramjet," NASA TM X-2895, Dec. 1973.

[3]Vinogradov, V. A., and Prudnikov, A. G., "Injection of Liquid into the Strut Shadow at Supersonic Velocities," Society of Automotive Engineers, SAE Paper 931455, April 1993.

[4]Livingston, T., Segal, C., Schindler, M., and Vinogradov, V. A., "Penetration and Spreading of Liquid Jets in an External–Internal Compression Inlet," AIAA Paper 99-2237, July 1999.

[5]Vinogradov, V. A., Kobigsky, S. A., and Petrov, M. D., "Experimental Investigation of Kerosene Fuel Combustion in Supersonic Flow," *Journal of Propulsion and Power*, Vol. 11, No. 1, 1995, pp. 130–134.

[6]Strokin, V. N., and Grachev, V. A., "The Peculiarities of Hydrogen Combustion in Scramjet Combustors," *Proceedings of the 13th ISABE Conference*, Vol. 1, Chattanooga, TN, AIAA, CP 9713, 1997, pp. 374–384.

[7]Tretyakov, P. K., Fomin, V. M., and Yakovlev, V. I., "New Control Principles of Aero-Physicals Processes. Development of Researches," *Proceedings of International Conference on Methods of Aero-Physical Researches*, Pt. 2, Novosibivsk, Russia, 1996, pp. 210–220.

[8]Goldfeld, M., Nestoulia, R., and Vinogradov, V., "Experimental Study of Scramjet Module," International Symposium on Air Breathing Engines, ISABE Paper IS-051, Sept. 1999.

[9]Bezgin, L., Ganzhelo, A. N., Gouskov, O. V., Kopchenov, V. I., Laskin, I., and Lomkov, K. E., "Numerical Simulation of Supersonic Flows Applied to Scramjet Duct," 1995, pp. 895–905.

[10]Gulyaev, A. V., Kozlov, V. E., and Secundov, A. N., et al., "Comparative Numerical Testing of One- and Two-Equation Turbulence Models for Flows with Separation and Reattachment," AIAA Paper 95-0863, Jan. 1995.

[11]Kopchenov, V. I., and Lomkov, K. E., "Enhancement of the Mixing and Combustion Processes Applied to Scramjet Engine," AIAA Paper 92-3428, July 1992.

[12]Godunov, S. K., Zabrodin, A. V., Ivanov, M. Ya., Kraiko, A. N., and Prokhopov, G. P., *Numerical Solution of Multi-Dimensional Gasdynamic Problems*, Nauka, Moscow, 1976 (in Russian).